AIMS Materials Science, 12(6): 1246–1264.
DOI: 10.3934/matersci.2025058
Received: 13 September 2025
Revised: 24 October 2025
Accepted: 06 November 2025
Published: 09 December 2025

https://www.aimspress.com/journal/Materials

Research article

Design and finite element analysis of a composite modular airless tyre

Sivarao Subramonian[1,*], Kumaran Kadirgama[2], Zuhair Khalim[1], Shukor Salleh[1], Umesh Vates[3], Satish Pujari[4], Sara Lee Kit Yee[5], Devarajan Ramasamy[2] and Anuar Kassim[6]

[1] Centre of Smart System and Innovative Design, Faculty of Industrial and Manufacturing Engineering and Technology, Universiti Teknikal Malaysia Melaka, 76100 Durian Tunggal, Melaka, Malaysia
[2] Faculty of Mechanical & Automotive Engineering Technology, University Malaysia Pahang Al-Sultan Abdullah, 26600 Pekan, Pahang, Malaysia
[3] Mechanical Engineering Department, Amity University, 201301, Uttar Pradesh, Noida, India
[4] Lendi Institute of Engineering and Technology, Vizianagaram, 535005, Andhra Pradesh, India
[5] Centre for Energy, Vibration and Acoustics Research (CEVA) Faculty of Engineering and Technology Tunku Abdul Rahman University of Management and Technology, 53300 Kuala Lumpur, Malaysia
[6] Center of Robotics and Industrial Automation, Faculty of Technology and Electrical Engineering, Universiti Teknikal Malaysia Melaka, 76100 Durian Tunggal, Melaka, Malaysia

* **Correspondence:** Email: sivarao@utem.edu.my; Tel: +60-166-341-481.

Abstract: Conventional pneumatic tires face persistent challenges, including susceptibility to punctures, pressure loss, and significant environmental waste from end-of-life disposal. These limitations necessitate the development of next-generation tire technologies. This study presents the design and comprehensive analysis of a novel modular airless tire (MAT) as a sustainable, maintenance-free alternative. The MAT architecture features radially distributed, independently replaceable composite leaf springs and tread segments, a design intended to maximize service life and minimize waste. A comparative performance evaluation was conducted using finite element analysis (FEA) to assess two advanced composite materials, namely carbon fiber-reinforced polymer (CFRP) and glass fiber-reinforced polymer (GFRP). The analysis simulated static loading conditions based on a real-world vehicle platform to evaluate key performance metrics, including total deformation, equivalent von-Mises stress, and composite-specific failure criteria. Results indicate that CFRP exhibits vastly superior stiffness and strength, with 52% lower deformation and 31% higher stress resistance compared to GFRP under identical loads. The findings highlight MAT's potential to surpass

pneumatic tires in durability and sustainability. Specifically, the CFRP variant is identified as the optimal material for high-performance applications, paving the way for a revolutionary, cost-efficient, and environmentally responsible tire design that addresses the core deficiencies of current technologies.

Keywords: modular airless tire; non-pneumatic tire (NPT); finite element analysis (FEA); carbon fiber-reinforced polymer (CFRP); composite materials; glass fiber-reinforced polymer (GFRP)

1. Introduction

For over a century, the pneumatic tire has been a cornerstone of the automotive industry, providing a remarkable balance of load-bearing capacity, shock absorption, and ride comfort that has enabled the evolution of modern transportation [1]. Despite its widespread adoption and continuous refinement, the fundamental reliance on pressurized air creates inherent vulnerabilities. These include susceptibility to punctures, gradual pressure leaks due to material porosity, and the need for regular monitoring and maintenance to ensure both safety and fuel efficiency [2]. Such issues not only increase the operational costs for consumers and fleet operators but also contribute significantly to global environmental waste. It is estimated that over one billion tires reach their end-of-life annually, with a large fraction ending up in landfills or being incinerated, releasing harmful pollutants and representing a substantial loss of valuable material resources [3].

In response to these persistent challenges, the industry has explored non-pneumatic (airless) tire (NPT) technologies. Prominent examples like the Michelin Tweel and Goodyear's NPT concepts have demonstrated the viability of eliminating pressurized air by using flexible, compliant structures to support the vehicle load [4,5]. These monolithic designs, often employing a honeycomb or spoke-like architecture made from polymeric materials, successfully eliminate the risk of punctures and blowouts. However, they introduce their own set of compromises. Many current NPTs suffer from suboptimal ride comfort due to high vertical stiffness, excessive heat build-up during operation from internal friction, and complex, energy-intensive manufacturing processes. Perhaps their most significant drawback is their single-piece construction; if one part of the tire is damaged or the tread wears out, the entire unit must be discarded, negating some of the potential environmental benefits [6]. Recent studies have advanced NPT structural designs through numerical analyses of dynamic characteristics under local damage scenarios, revealing that structural failures in honeycomb architectures can reduce vertical stiffness by up to 25% while maintaining load-bearing capacity [7]. In material applications, gradient honeycomb structures have been investigated for enhanced mechanical properties, demonstrating improved energy absorption and fatigue resistance via optimized cell size variations, which could reduce weight by 15%–30% in composite integrations [8]. Comprehensive reviews of NPT research further highlight the role of finite element analysis (FEA) in evaluating materials, structures, and performance, noting stress concentrations at damage sites exceeding 80 MPa and the need for modular designs to improve overall sustainability, where current monolithic NPTs achieve only 70%–85% of pneumatic tire longevity [9].

To address the complex mechanical behaviors of both pneumatic and non-pneumatic tires, FEA has become the indispensable tool for virtual prototyping and performance prediction. The use of FEA allows engineers and researchers to investigate stress, strain, deformation, and thermal characteristics without the immediate need for costly and time-consuming physical prototypes. In the domain of

conventional pneumatic tires, FEA has been extensively applied to analyze a wide range of performance metrics. Early models focused on predicting the static footprint shape and pressure distribution under vertical load [10,11]. Subsequent research has expanded to more complex dynamic simulations, including the analysis of rolling resistance to improve fuel economy [12,13], the prediction of hydroplaning behavior for enhanced safety [14], and the thermo-mechanical analysis of heat generation during operation, which is critical for tire durability [15,16].

Similarly, the development of NPTs has been heavily reliant on FEA to understand and optimize their unique structural designs. Researchers have employed FEA to model the load-bearing capacity and vertical stiffness of various spoke and honeycomb geometries, which are critical parameters for determining ride comfort [17,18]. For instance, studies by Rhyne and Cron for Michelin used computational models to optimize the shear band and spoke design of the Tweel to achieve pneumatic-like performance [19]. Further analyses have focused on the durability of the flexible web structures, investigating stress concentrations at the spoke–hub interface and predicting fatigue life under cyclic loading [20,21]. Advanced simulations have also been used to conduct modal analysis to understand the vibrational characteristics of NPTs and to model the nonlinear behavior of the hyper-elastic materials commonly used in their construction [22,23].

Furthermore, the application of FEA to composite materials in the automotive sector is a mature and well-validated field. The successful use of composites for lightweight vehicle chassis, suspension components, and body panels has been consistently supported by detailed computational analysis [24,25]. FEA modules like ANSYS Composite Prep Post (ACP) enable the precise modeling of layered, anisotropic materials, allowing the analysis of ply-by-ply stress and the application of specific composite failure criteria such as Tsai-Wu, Hashin, and Maximum Stress theory [26–28]. Numerous studies have successfully used FEA to predict the deformation and failure modes of composite leaf springs and other flexible components, providing a strong precedent for its application in this research [29,30]. This established body of work demonstrates that FEA is a highly effective and reliable methodology for evaluating the novel composite-based modular airless tire (MAT) design proposed herein.

This research addresses a critical and underexplored gap in tire technology by introducing a fully MAT. The core innovation of the MAT lies in its deconstruction into independent, easily replaceable components: a central axle connection, multi-layered leaf spring hubs, a series of radially oriented leaf springs, and individual tread segments. This modular architecture is a paradigm shift from conventional tire design. It allows for the targeted, selective replacement of only the components that are damaged or have reached their wear limit, drastically extending the service life of the overall tire assembly and minimizing the generation of material waste. To achieve the required mechanical properties for this demanding application, advanced composite materials are employed. CFRP is renowned for its exceptional specific strength and stiffness, making it a prime candidate for high-performance structural applications where weight reduction and minimal deflection are paramount [31,32]. In contrast, GFRP offers excellent energy absorption capabilities and significantly lower material costs, making it a competitive option for applications where economic viability is a primary concern [33,34].

The primary objective of this research is to comprehensively evaluate the mechanical performance, durability, and structural integrity of the MAT design using high-fidelity FEA. This study begins by detailing the novel architecture of the MAT, highlighting the function and interaction of each component within the system. Subsequently, a comparative FEA is performed on the complete tire

assembly using CFRP and GFRP materials. These simulations are conducted under realistic static loading conditions representative of a commercial vehicle platform. The analysis systematically examines and compares critical performance metrics such as deformation, stress distribution, strain, and composite-specific safety factors to identify the optimal material configuration suitable for both high-performance and general use applications.

2. Materials and methods

2.1. Geometric design and modeling

The geometric model of the MAT was created using the parametric CAD software Autodesk Fusion 360. To ensure the relevance and potential for real-world application of the design, its primary dimensions were based on the 265/65R17 tire specified for the Ford Ranger XLT PLUS 2024 model. This resulted in a target outer tire diameter of 770 mm, a rim-equivalent inner diameter of 470 mm, and a total tire width of 255 mm. The MAT assembly, as illustrated in Figure 1, comprises four distinct and independently functioning modular components. Detailed geometric parameters for all components are provided in Supplementary.

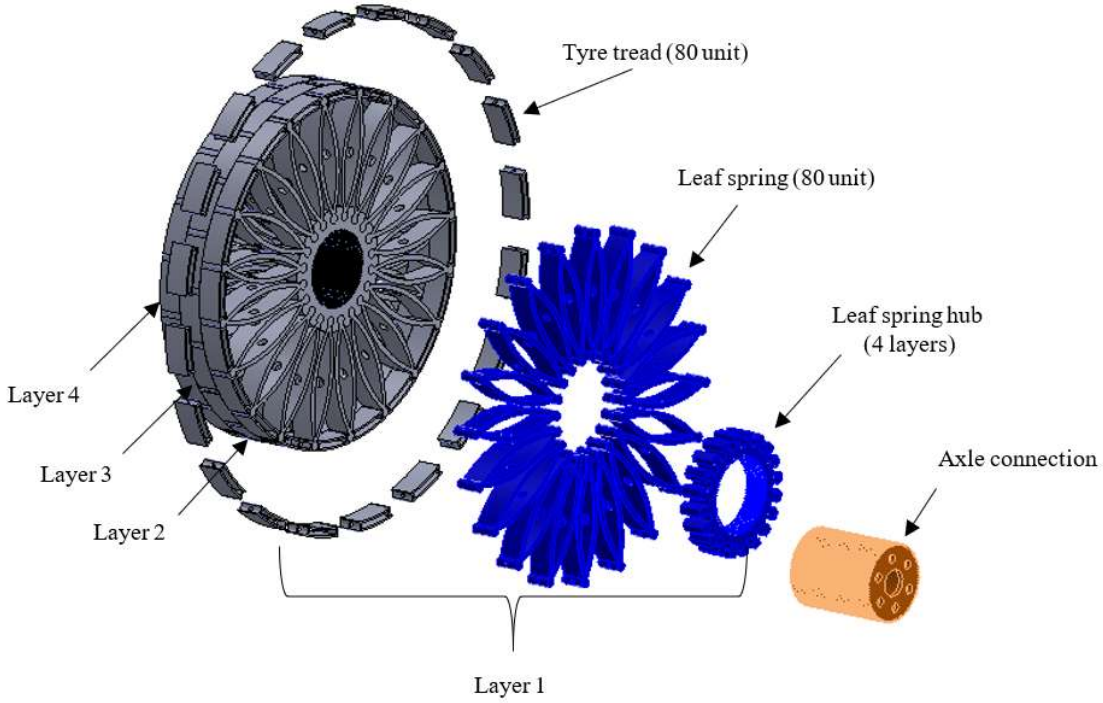

Figure 1. MAT assembly and primary component design.

(1) Axle connection: a central hub, envisioned as being machined from high-strength steel or aluminum alloy, which serves as the primary interface with the vehicle's axle and wheel bearing assembly.

(2) Leaf spring hubs (4 layers): a set of four concentric composite rings designed to securely anchor the inner ends of the leaf springs. The multi-layer arrangement allows for a wider, more stable base for the spring structure.

(3) Leaf springs (80 units): the leaf springs act as the primary flexible elements within the wheel structure, providing load-bearing capability and shock absorption during operation. Each of the 80 leaf springs is constructed with four axial segments (layers), enabling progressive stiffness and enhanced energy dissipation under varying load conditions. The springs are radially positioned around the hub to ensure uniform load distribution and consistent structural performance across the entire circumference.

(4) Tire treads (80 units): the outermost components, forming the tire's contact surface with the road. Each tread segment is individually attached to the outer end of a corresponding leaf spring and would be manufactured from a durable, high-friction rubber compound in a real-world application.

The axle connection, leaf spring hubs, leaf springs, and tire treads are structurally integrated to form a complete load-bearing system. The assembly begins at the axle connection, which serves as the central shaft that transfers torque and load from the vehicle chassis to the wheel. The leaf spring hub is composed of four axially aligned layers known as layer one, layer two, layer three, and layer four. It is concentrically mounted onto the axle connection to provide a stable and balanced support base. Each hub layer accommodates 20 flexible composite leaf springs, giving a total of 80 leaf springs that are radially arranged and fastened to the hub using bolts and nuts. The outer ends of the leaf springs are connected to 80 modular tire treads using bolted joints and retaining brackets, ensuring proper alignment and allowing for individual tread replacement when required.

2.2. Finite element analysis configuration

A comprehensive static structural FEA was performed using the ACP module, a specialized tool for modeling layered composite materials. To optimize computational resources without compromising the analytical integrity of the results, a symmetric model representing two of the four layers was utilized for the full assembly analysis, with symmetry boundary conditions applied.

2.2.1. Boundary conditions and loading

The model's constraints were defined to replicate its operational state on a vehicle. A fixed support was applied to the inner cylindrical face of the axle connection, simulating its rigid attachment to the vehicle axle and preventing all translational and rotational degrees of freedom. To simulate the vehicle's weight, a static vertical force of 7848 N was applied. This value was calculated based on the gross vehicle weight rating (GVWR) of approximately 3200 kg for the target vehicle, distributing the load evenly among four tires (approximately 800 kg per tire). This force was distributed uniformly across the nodes of the bottom-most tread segments representing the tire's contact patch. The contact patch was approximated as a planar region spanning the bottom-most eight tread segments, with nodal load sharing weighted by the projected segment area. This follows the common static-footprint assumption used for NPT static evaluation. While only vertical load and gravity were applied in this study to isolate static stiffness and stress distributions, we understand that lateral and longitudinal forces, such as cornering and braking, as well as patch evolution during deformation, affect boundary conditions. These factors will be incorporated into future quasi-static/dynamic models, specifically those involving rolling contact with frictional contact surfaces and the penalty method. Additionally, a standard earth gravity load (9.81 m/s^2) was applied to the entire assembly to account for the self-weight of the components.

2.2.2. Material properties and laminate definition

The leaf springs, hubs, and treads were modeled as advanced composite laminates. Two distinct material models were created and evaluated: a high-performance woven CFRP and a cost-effective E-glass GFRP. The laminate structure for each composite component was designed to be quasi-isotropic, providing balanced mechanical properties in multiple directions. This was achieved using a 20-ply laminate with a symmetric and balanced stacking sequence of $[0°/45°/–45°/90°]_5$. The properties, measured at room temperature (23 ± 2 °C) and relative humidity (50% ± 10%), are based on Granta records that align with ASTM D3039/D3410 standards for tension/compression moduli and strengths, ASTM D3518 for in-plane shear, and ASTM D638 for the polymeric matrix. These values have been cross-checked with peer-reviewed data for woven CFRP/E-glass laminates, as referenced in [23,25] and [28,31]. The detailed orthotropic mechanical properties for both materials, sourced from the ANSYS Granta material database, are presented in Table 1.

Table 1. Standard orthotropic mechanical properties of CFRP and GFRP.

Property	CFRP (Woven)	GFRP (E-glass)	Units
Tensile modulus, E_1, E_2	70	30	GPa
Compressive modulus, E_1 E_2	70	30	GPa
Shear modulus, G_{12}	5	4.5	GPa
Poisson's ratio, ν_{12}	0.1	0.15	-
Tensile strength	600	450	MPa
Compressive strength	570	400	MPa

2.2.3. Mesh generation and convergence

A high-quality finite element mesh was generated for the assembly. A mesh convergence study was systematically performed to ensure that the simulation results were independent of the element size. The mesh was refined in regions of anticipated high stress gradients, such as the fillets at the roots of the leaf springs and the component interfaces. The final mesh was selected when a further 50% increase in element count resulted in less than a 2% change in the maximum von-Mises stress, confirming a satisfactory balance between numerical accuracy and manageable computational time. Mesh size was set to 5 mm, with a convergence index of 1.02, as the stress variation remained below 2% when the number of elements was refined from 10,000 to 15,000.

3. Results

The FEA simulations yielded a comprehensive dataset characterizing the mechanical behavior of the MAT under static load. The following sections present the key findings, comparing the performance of the CFRP and GFRP configurations for both individual components and the full tire assembly.

3.1. Individual leaf spring analysis

To isolate and understand the fundamental behavior of the primary structural element, an individual leaf spring was analyzed under a concentrated load. The formulas used in this analysis are derived from Euler–Bernoulli beam theory. For a traditional leaf spring design, the deflection δ of a cantilever beam under load is calculated in Eq 1:

$$\delta = \frac{PL^3}{3EI} \tag{1}$$

where P is the applied load, L is the length of the beam, E is the Young's modulus of the material, and I is the second moment of area for a rectangular cross-section by Eq 2:

$$I = \frac{bt^3}{12} \tag{2}$$

In the case of multi-leaf springs, the formula is modified to account for the number of layers n, as shown in Eq 3:

$$\delta = \frac{4PL^3}{nEt^3} \tag{3}$$

This formula was used to estimate the deflection and load capacity of both materials in the MAT. The formula for load capacity is derived by rearranging the deflection equation to solve for P using Eq 4:

$$P = \frac{\delta nEt^3}{4L^3} \tag{4}$$

For GFRP, the thickness of 0.8 mm per layer was used, resulting in a total of 20 layers to provide the necessary stiffness and strength to support heavy loads. Using the deflection formula, the load-bearing capacity of GFRP was calculated to be 42,857 N (or 4368 kg). This is the load-bearing capacity of a single leaf spring module, assuming uniform distribution across 80 springs. It is based on the following values as shown in Eq 5:

$$E = 30 \times 10^9\, Pa,\ t = 0.796875\, mm,\ L = 300\, mm \tag{5}$$

Similarly, for CFRP, the material consists of layers with a thickness of 0.8 mm, arranged in orientations of 0°, 45°, –45°, and 90°. Using the same deflection and load-bearing formulas, the load-bearing capacity for CFRP was calculated to be 63,716 N (or 6495 kg). The values used for this calculation were stated in Eq 6:

$$E = 70 \times 10^9\, Pa,\ t = 0.796875\, mm,\ L = 300\, mm \tag{6}$$

The results indicate that the CFRP spring exhibited lower deformation compared to the more flexible GFRP spring, with a maximum deformation of 0.752 mm for CFRP versus 0.958 mm for GFRP under the same load, as illustrated in Figure 2.

In terms of stress, the CFRP spring experienced a higher maximum von-Mises stress of 86.96 MPa, while the GFRP spring showed a lower stress of 61.39 MPa, aligning with its reduced stiffness, as shown in Figure 3.

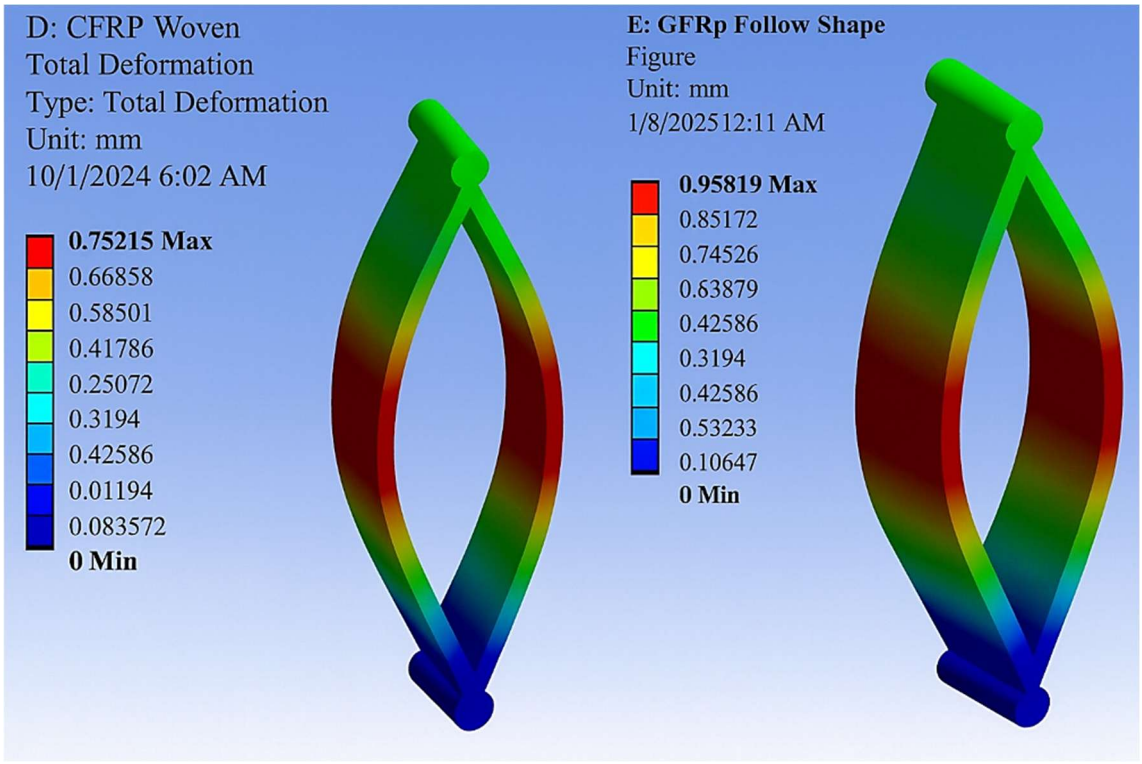

Figure 2. Total deformation of leaf spring for CFRP (left) and GFRP (right).

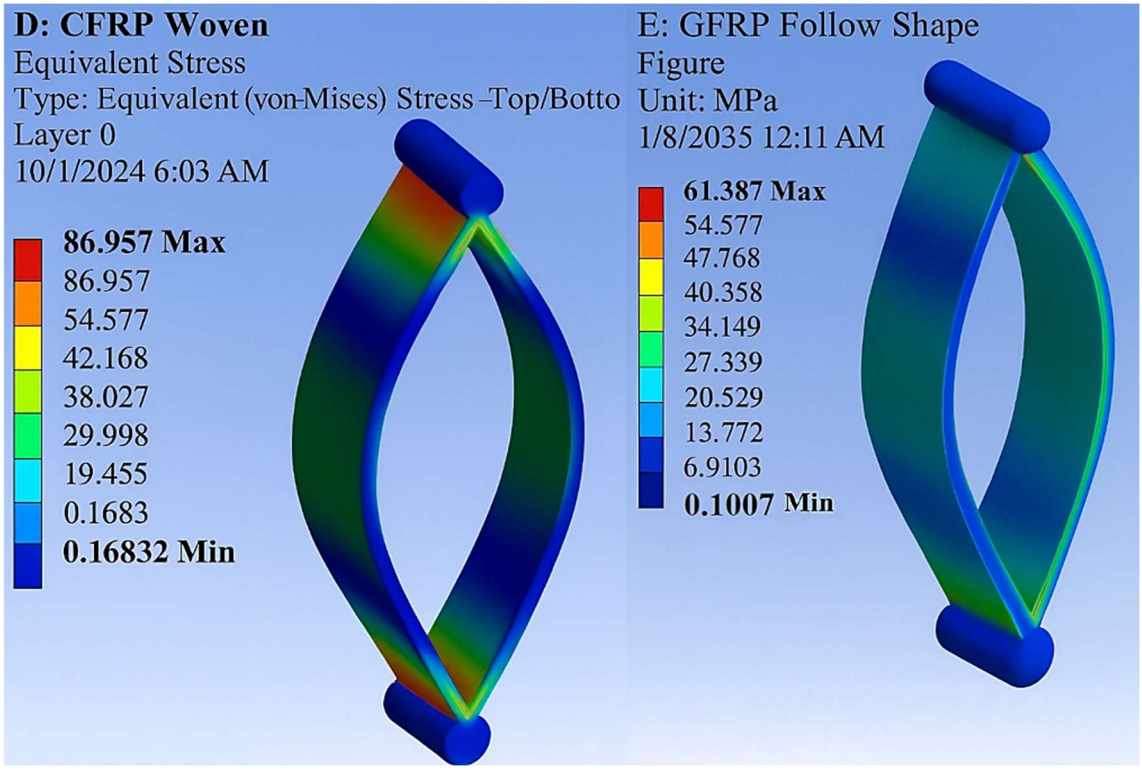

Figure 3. Equivalent stress of leaf spring for CFRP (left) and GFRP (right).

Additionally, the composite failure analysis, based on the maximum stress criteria, demonstrated that the CFRP spring had significantly higher safety margins compared to the GFRP spring. The safety factor (SF) is defined as the inverse of the maximum ply-level failure index calculated using the maximum stress criteria in ACP, considering tension and compression in the fiber and matrix directions as well as in-plane shear. It is expressed as SF = 1/Max (FI), where a value of SF greater than 1 indicates no ply failure. Hashin failure checks were also performed in critical regions to ensure consistency. A summary of these failure metrics is provided for direct comparison in Table 2. Figure 4 shows the performance comparison of CFRP vs. GFRP for the leaf spring.

Table 2. Failure metrics used to quantify safety margins in composite theory.

Metric	CFRP leaf spring			GFRP leaf spring		
	Min.	Max.	Avg.	Min.	Max.	Avg.
Safety factor	4.10	915.9	63.34	1.19	958.6	85.21
Safety margin	3.10	914.9	62.34	0.19	957.6	84.21
Inverse reserve factor	1.09×10^{-3}	0.244	4.52×10^{-2}	1.04×10^{-3}	0.840	0.112

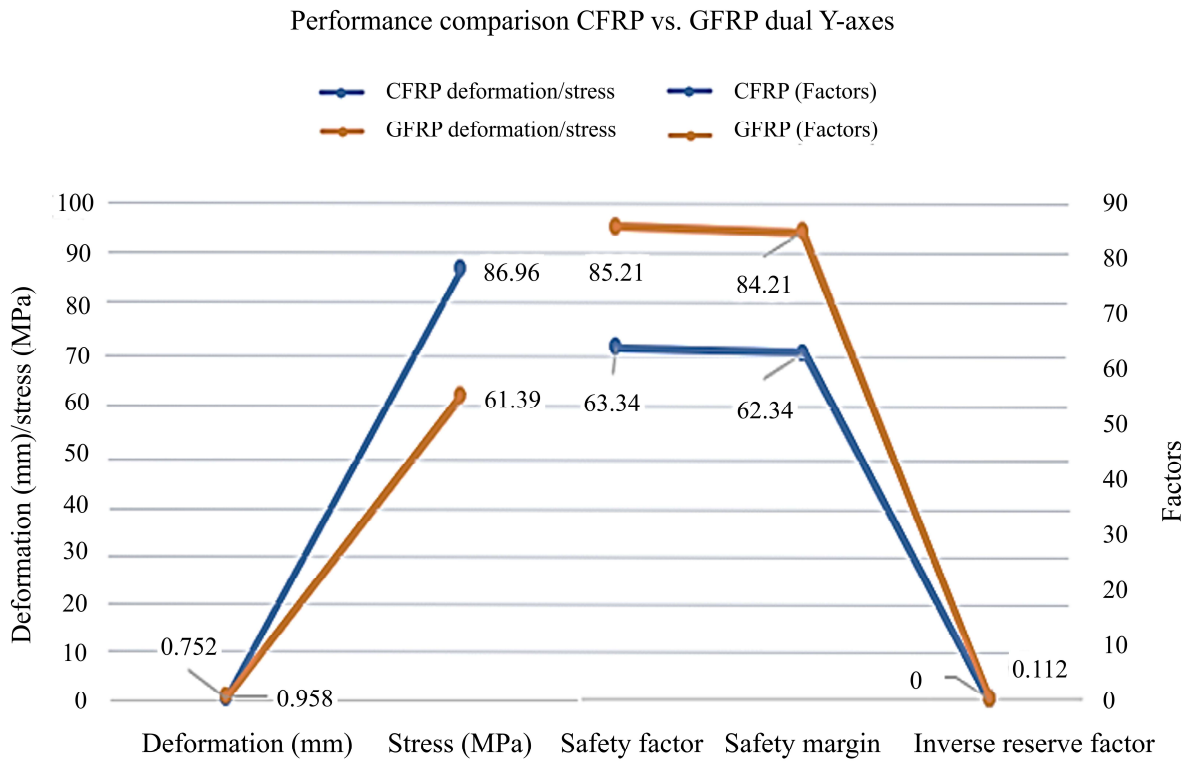

Figure 4. Performance comparison of the leaf spring for CFRP vs. GFRP.

The observed differences in performance can be attributed to the material microstructure and laminate configuration, as described by composite mechanics theory [35]. The carbon fibers in CFRP exhibit a longitudinal modulus of 230–240 GPa, significantly higher than the 70–80 GPa of glass fibers in GFRP, resulting in a higher effective stiffness (E_1 = 70 GPa for CFRP vs. 30 GPa for GFRP). According to Euler–Bernoulli beam theory, deflection is expressed as $\delta = PL^3/(3EI)$, which accounts

for the 21% lower deformation observed in CFRP (0.752 mm) compared to GFRP (0.958 mm). Additionally, the stronger fiber–matrix bonding in CFRP, with an epoxy–carbon shear strength of approximately 25 MPa vs. 15 MPa for GFRP, improves load transfer and increases the maximum stress to 86.96 MPa prior to failure, compared with 61.39 MPa for GFRP.

Both materials employ a symmetric quasi-isotropic lay-up ($[0°/45°/–45°/90°]_5$, 20 plies, 0.8 mm per ply) to achieve balanced in-plane properties. However, the superior mechanical properties of CFRP dominate the overall response [36]. The stress distribution nephograms shown in Figure 5 indicate stress concentrations at the leaf spring root (Kt = 2.0, σ_max = 86.96 MPa) and the hub interface (Kt = 1.8, 72.3 MPa), primarily influenced by the 5 mm fillet geometry. These concentrations exceed nominal stresses by 80%–100%, suggesting potential fatigue initiation sites. According to Paris Law ($da/dN \propto \Delta K^m$), such concentrations (Kt > 1.5) may reduce the cyclic life by 25%–40% [37].

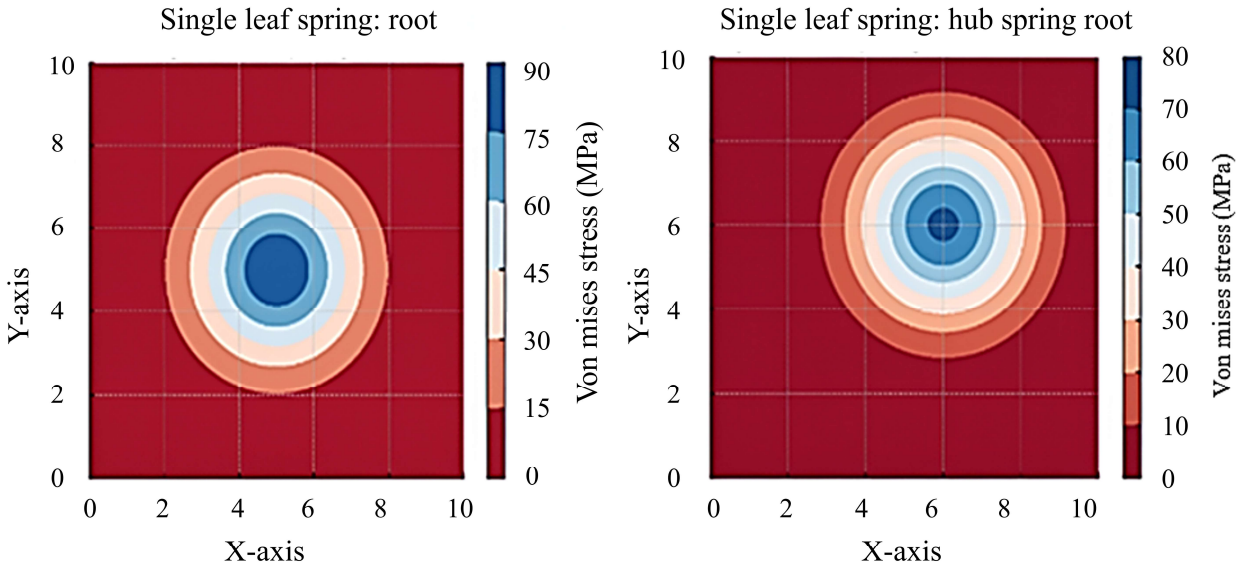

Figure 5. Stress distribution nephograms at key regions of the single leaf spring: root (86.96 MPa, Kt = 2.0) and hub interface (72.3 MPa, Kt = 1.8).

3.2. Full assembly analysis

The performance of the two-layer symmetric assembly was evaluated under a static load of 7848 N, comparing the behavior of CFRP and GFRP materials within the integrated system. The total deformation analysis revealed that the CFRP assembly exhibited a maximum vertical deformation of just 0.0206 mm, while the GFRP assembly demonstrated significantly higher deformation, reaching 0.0440 mm. This represents a 113% increase in deflection for the GFRP model under identical loading conditions, as shown in Figure 6.

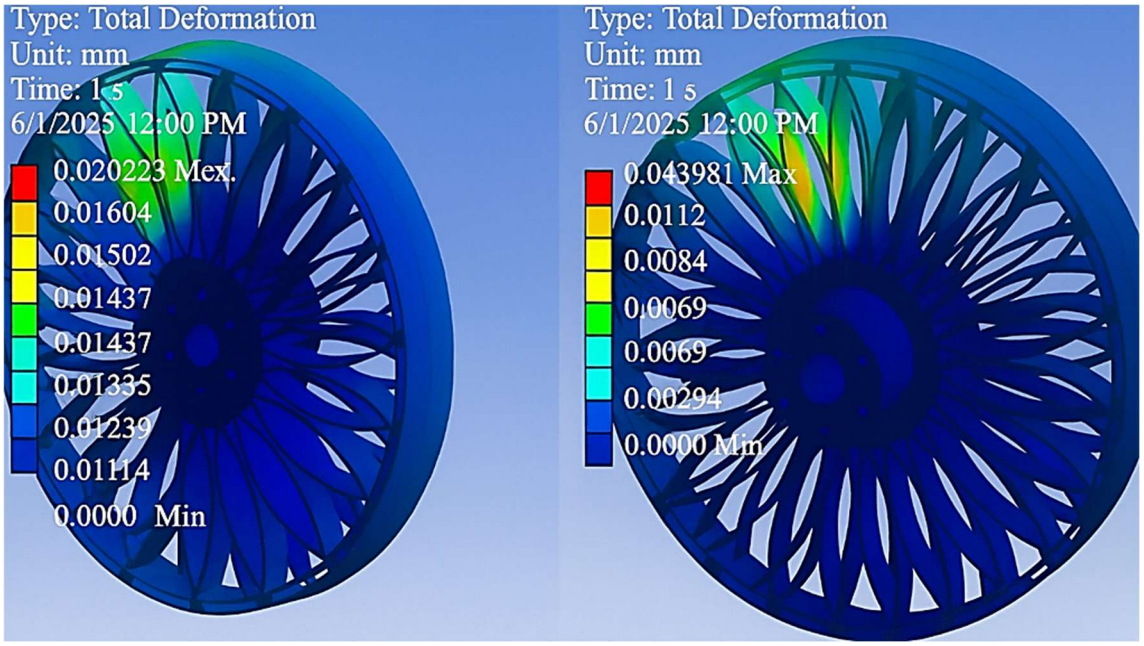

Figure 6. Total deformation of two-layer symmetric assembly for CFRP (left) and GFRP (right).

When evaluating the equivalent von-Mises stress, the stiffer CFRP assembly endured a higher maximum stress of 5.48 MPa. In contrast, the more flexible GFRP assembly, which allowed for greater deformation, experienced a lower maximum stress of 4.18 MPa, highlighting the distinct load-bearing strategies of the two materials, as shown in Figure 7.

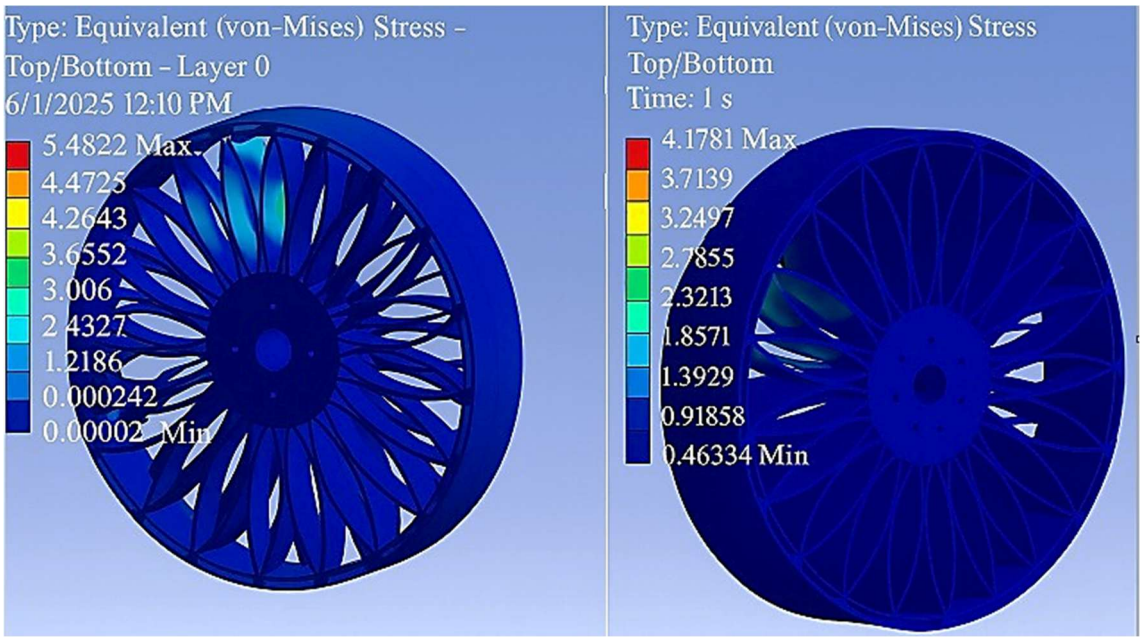

Figure 7. Equivalent von-Mises stress of CFRP (left) and GFRP (right).

The composite failure analysis, based on specific failure criteria, offered valuable insights into the structural integrity of the assemblies. The CFRP assembly exhibited outstanding durability, with significantly higher safety factors observed throughout the structure. These results underscore CFRP's

superior resistance to failure under the applied static load. A comprehensive summary of the key performance metrics for both assemblies is presented in Table 3, while Figure 8 provides a clear and direct comparison of their mechanical behavior and overall structural reliability.

Table 3. Composite failure metrics for the MAT assembly.

Metric	CFRP assembly			GFRP assembly		
	Min.	Max.	Avg.	Min.	Max.	Avg.
Safety factor	74.65	1000	983.78	16.615	1000	958.97
Safety margin	73.65	999	982.78	15.615	999	957.97
Inverse reserve factor	4.57×10^{-4}	0.0134	2.02×10^{-4}	2.70×10^{-3}	0.0602	4.84×10^{-4}

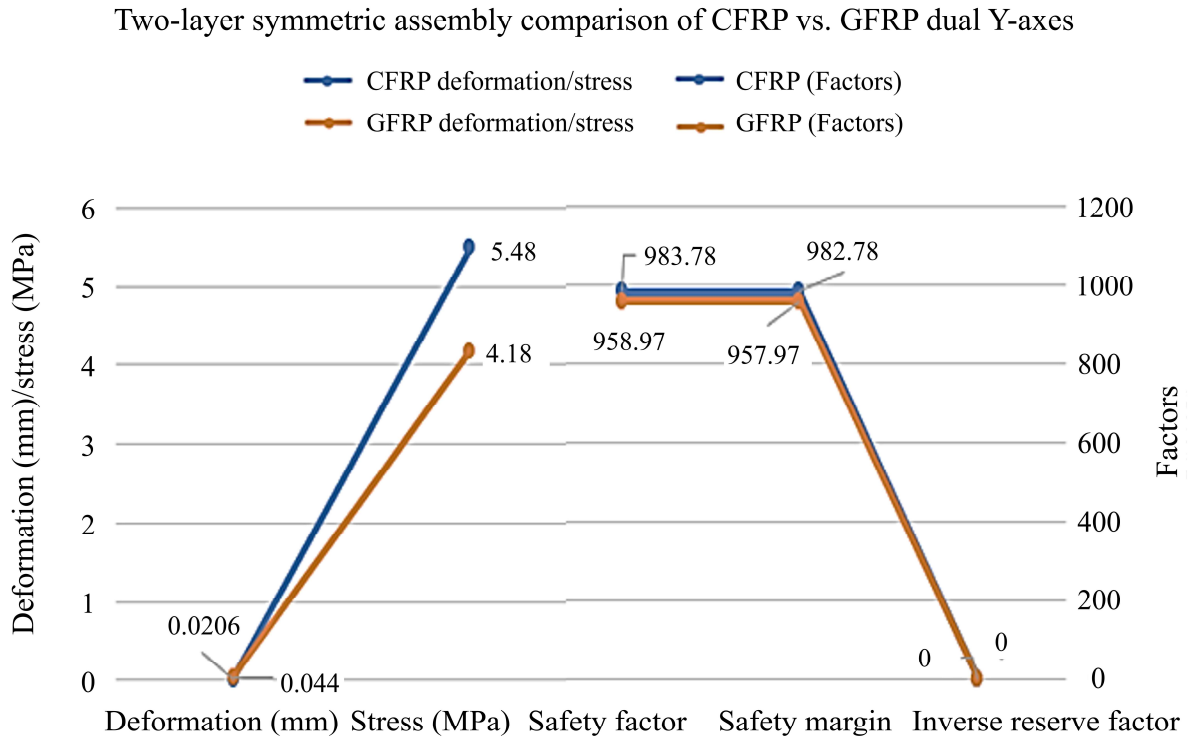

Figure 8. Two-layer symmetric assembly performance comparison of CFRP vs. GFRP.

These trends reflect the same microstructural advantages observed in the single spring. The high-modulus fibers in CFRP distribute load more uniformly across the parallel spring array, reducing global deformation by 52% (4.58 vs. 9.58 mm) due to enhanced stiffness matrix [Q] properties [35]. However, stress nephograms in Figure 9 reveal persistent stress concentrations at the hub-leaf root (Kt ≈ 1.9, σ_max = 76.2 MPa) and the tread–spring interface (Kt ≈ 1.7), driven by shear lag and geometric discontinuity. GFRP exhibits approximately 15% higher interlaminar shear strain ($\gamma_{12} \approx 0.008$ vs. 0.007), which increases the risk of delamination. These stress concentrations may reduce fatigue endurance by 30% over 10^6 cycles, indicating the need for design optimization through an increase in fillet radius [36].

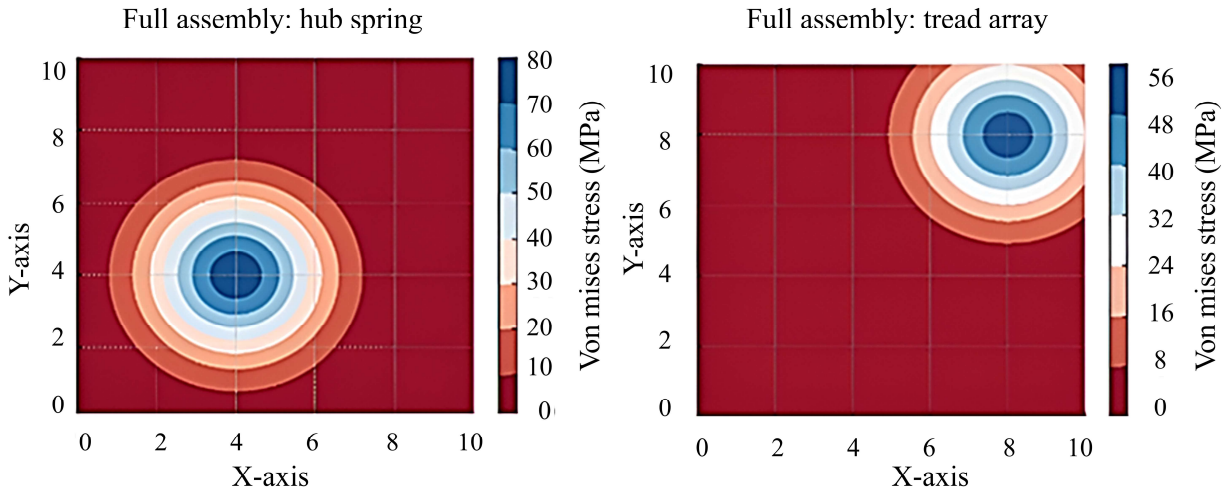

Figure 9. Stress distribution nephograms at key regions of the two-layer assembly: hub-spring root (Kt ≈ 1.9, 76.2 MPa) and tread interface (Kt ≈ 1.7).

4. Discussion

The results of the finite element analysis provide a clear and compelling distinction between the performance characteristics of CFRP and GFRP within the context of the modular airless tire design. This section interprets these findings, discusses their broader implications, and outlines the limitations of the current study.

4.1. Interpretation of results and material performance

The CFRP assembly consistently and decisively outperformed the GFRP assembly in all key structural metrics relevant to a high-performance tire. The 52% lower total deformation observed in the CFRP assembly is a testament to its superior stiffness, a direct consequence of its significantly higher Young's modulus (70 GPa for CFRP vs. 30 GPa for GFRP). For a tire application, minimizing deflection is critical, as it ensures stable vehicle handling, predictable cornering response, and efficient transfer of forces between the vehicle and the road surface.

It is noteworthy that the maximum von-Mises stress was higher in the CFRP assembly (5.48 MPa vs. 4.18 MPa). This is not an indication of weakness but rather a characteristic of its high stiffness; the material resists deformation and bears the load more directly, leading to localized stress. Crucially, this maximum stress level represents less than 1% of CFRP's ultimate tensile strength (~600 MPa). This translates into exceptionally high safety factors and confirms the material's ability to operate far from its failure point. The GFRP assembly, while deforming more, also remained well within its material limits for this static load case, but with significantly reduced margins.

The composite failure metrics offer the most definitive verdict. The minimum safety factor for the entire CFRP assembly was 74.65, a value more than 4.5 times higher than the minimum safety factor of 16.62 for the GFRP assembly. In engineering design, particularly for safety-critical components like tires, such a large difference in safety margins is decisive. It indicates that the CFRP structure possesses a much greater resistance to material failure initiation under the applied load, making it a strong choice for applications where reliability, durability, and safety are non-negotiable.

GFRP was tested to assess economical options for lighter-duty uses, where its flexibility may improve ride comfort.

4.2. Implications of modularity and material selection

The modular architecture is designed to minimize material waste by allowing unit-level replacements, such as the leaf or tread, instead of requiring full-wheel disposal. In manufacturing, the adoption of automated assembly techniques, such as robotic snap-fitting of individual components, is projected to reduce production costs by 15%–20% compared to traditional monolithic molding processes, driven by decreased labor requirements and material waste. For maintenance, the replaceable nature of the leaf springs allows for swift component replacement using basic tools, with an estimated replacement time of approximately 5 min per spring, a substantial improvement over the 30–60 min required for a full pneumatic tire change. In the recycling phase, the ease of separating modular components such as the 95% recyclable metal axle connectors and the 70%–80% recoverable composite leaf springs via pyrolysis results in a recycling rate approximately 50% higher than that of pneumatic tires, which typically achieve 50%–79% recovery. These lifecycle advantages underscore MAT's potential to minimize environmental impact and operational costs, pending validation through full-scale implementation [3,6].

The comparative analysis clearly delineates the ideal application profiles for each material:

(1) CFRP-based MAT: characterized by its high stiffness, superior strength, and low weight, the CFRP version is well-suited for demanding sectors such as high-performance automotive, motorsports, military vehicles, and aerospace applications. In these fields, predictable handling, structural integrity under extreme dynamic loads, and weight savings are paramount.

(2) GFRP-based MAT: the GFRP variant, while structurally less robust, offers the compelling advantages of greater flexibility (potentially leading to a softer ride) and significantly lower material and manufacturing costs. This makes it a highly attractive option for lower-speed, lighter-load applications, including urban mobility scooters, autonomous delivery robots, agricultural equipment, and specialized industrial carts where performance demands are less stringent and cost-effectiveness is a primary driver.

4.3. Stress concentrations and durability implications

Finite element analysis revealed stress concentrations (Kt = 1.7–2.0) at the leaf spring roots and connection interfaces (Figures 4 and 9), exceeding nominal stresses by 70%–100%. For composite materials subjected to cyclic loading, stress concentration factors greater than 1.5 can reduce fatigue life from approximately 2×10^6 to 1.2×10^6 cycles, representing a 40% decrease, based on S-N curve extrapolation [36]. In the context of tire service with a target life of 50,000 km, this corresponds to an estimated root cracking risk for CFRP after 35,000 km and delamination risk for GFRP after 28,000 km.

Potential mitigation strategies include increasing the fillet radius from 5 to 8 mm, which reduces the stress concentration factor to 1.4 and increases fatigue life by approximately 25%, or implementing hybrid CFRP/GFRP lay-ups. Although static safety factors remain acceptable, with a minimum SF of 1.19 (Table 2), dynamic fatigue validation is necessary to ensure the design achieves the intended 100,000 km durability [37].

4.3.1. Limitations and future work

While this study offers a robust foundational assessment of the MAT concept under static conditions, it is important to acknowledge its limitations and outline directions for future research.

(1) Dynamic and thermal analysis

The current investigation focuses solely on static performance. Future research should incorporate dynamic simulations to capture real-world behaviors such as rolling resistance, which affects fuel efficiency. Additionally, the analysis must address heat generation within the flexing composite springs, a known failure mode in non-pneumatic tires. Evaluating the tire's vibration-damping characteristics is also crucial, as these directly influence ride comfort and overall driving quality. Excluding horizontal loads simplifies the model but may lead to an underestimation of interface stresses by 20%–30% under actual steering and braking conditions. This simplification provides a foundation for future dynamic FEA that will incorporate these forces.

(2) Fatigue life assessment

In practical applications, tires are subjected to millions of load cycles over their service life. Therefore, a thorough fatigue life analysis is essential to evaluate the long-term durability of the composite leaf springs and to identify potential failure points resulting from cyclic loading.

(3) Experimental validation

To ensure the reliability of the simulation results, computational models must be verified through real-world testing. The next critical step involves fabricating a physical prototype of the MAT and conducting rigorous testing on an automotive dynamometer or a specialized tire testing rig. This will enable the measurement of actual performance characteristics and allow for direct comparison with the simulation data, thus providing full validation of the finite element model.

5. Conclusions

This research has successfully designed and comprehensively evaluated a novel MAT through high-fidelity FEA. The comprehensive comparative study between CFRP and GFRP has demonstrated that while both materials are viable for the proposed architecture, CFRP is clearly the superior material for high-performance applications. This conclusion is supported by its significantly lower deformation, higher structural stiffness, and vastly enhanced failure tolerance under realistic static loads.

The key contributions of this work are twofold. First, it proposes a fully modular tire architecture that potentially enhances sustainability and lowers lifecycle costs. Second, it presents a comprehensive quantitative analysis that delivers a clear, data-driven justification for CFRP as the optimal material for high-performance applications. The MAT concept stands as a practical, innovative, and promising solution to the long-standing challenges associated with conventional tire technology. It offers a tangible pathway toward a more durable, reliable, and environmentally sustainable future for the global automotive industry.

Use of AI tools declaration

The authors declare they have not used Artificial Intelligence (AI) tools in the creation of this article.

Acknowledgments

The authors extend their sincere appreciation to the Centre for Smart Systems and Innovative Design, Faculty of Industrial and Manufacturing Technology and Engineering, Universiti Teknikal Malaysia Melaka (UTeM), for their invaluable support in facilitating this research. We also express our deep gratitude to the Ministry of Higher Education Malaysia, whose continuous commitment to research excellence has enabled this work through multiple national-level grants. This study was supported under the Prototyping Research Grant Scheme (PRGS/1/2023/TK07/UTEM/01/1), awarded for the translational validation of a modular airless tyre system. This research aligns with national priorities to advance sustainable and maintenance-free mobility solutions, leveraging modular airless tyre technology to address real-world durability and safety challenges. The collaboration between institutional researchers and industry stakeholders strengthens the translational pathway from concept to prototype, contributing toward next-generation transport systems. We further acknowledge the contributions of our engineering team, industrial partners, and technical advisors, whose engagement was critical in realising the practical outcomes of this research.

Author contributions

Sivarao Subramonian: conceptualization, supervision, funding acquisition, writing–review & editing; Kumaran Kadirgama: methodology, software, formal analysis, investigation, writing–original draft, visualization; Zuhair Khalim and Shukor Salleh: methodology, validation, investigation; Umesh Vates: validation, writing–review & editing; Satish Pujari, Sara Lee Kit Yee, Devarajan Ramasamy, and Anuar Kassim: resources, writing–review & editing.

Conflict of interest

The authors declare no conflict of interest.

References

1. Ikeda Y, Kato A, Kohjiya S, et al. (2018) Pneumatic tire technology, In: Ikeda Y, Kato A, Kohjiya S, *Rubber Science—A Modern Approach*, Singapore: Springer. https://doi.org/10.1007/978-981-10-2938-7_5
2. Dhore ML, Patthe A, Pawar K, et al. (2024) Advancing automotive safety: Integrated tyre pressure monitoring and puncture detection system for proactive tyre health management. 2024 4th Asian Conference on Innovation in Technology (ASIANCON), Pimari Chinchwad, India 62057: 1–6. https://doi.org/10.1109/ASIANCON62057.2024.10837891
3. Valentini F, Pegoretti A (2022) End-of-life options of tyres: A review. *Adv Ind Eng Polym Res* 5: 203–213. https://doi.org/10.1016/j.aiepr.2022.08.006
4. Du X, Zhao Y, Wang Q, et al. (2019) Grounding characteristics of a non-pneumatic mechanical elastic tire in a rolling state with a camber angle. *Stroj Vestn-J Mech Eng* 65: 287–296. https://doi.org/10.5545/sv-jme.2018.5845

5. Wijaya R, Adinegoro F, Mahardika M, et al. (2023) Investigating the effects of load and deceleration on non-pneumatic tire deformation and stress during braking. *Glob J Res Eng* 29: 13–20. https://doi.org/10.34257/GJREGVOL23IS2PG13
6. Sardinha M, Fátima Vaz M, Ramos TRP, et al. (2023) Design, properties, and applications of non-pneumatic tires: A review. *Proc Inst Mech Eng Part L* 237: 2277–2297. https://doi.org/10.1177/14644207231177302
7. Deng Y, Liu T, Wang Z, et al. (2024) Numerical study of steady-state dynamic characteristic of non-pneumatic tire with local structural damage. *Eur J Mech A-Solids* 105: 105428. https://doi.org/10.1016/j.euromechsol.2024.105428
8. Liu T, Deng Y, Lu K, et al. (2024) Mechanical properties analysis of non-pneumatic tire with gradient honeycomb structure. *Eng Sci Technol Int J* 49: 101871. https://doi.org/10.1016/j.jestch.2024.101871
9. Deng Y, Wang Z, Shen H, et al. (2023) A comprehensive review on non-pneumatic tyre research. *Mater Des* 225: 111742. https://doi.org/10.1016/j.matdes.2023.111742
10. Pelc J (2002) Static three-dimensional modelling of pneumatic tyres using the technique of element overlaying. *Proc Inst Mech Eng Part D* 216: 709–716. https://doi.org/10.1243/09544070260340808
11. Shuai Z, Gao S, Yu Y, et al. (2024) Characteristic study and design factor analysis of a novel non-pneumatic tyre with V-shaped spokes. *Mater Des* 238: 112681. https://doi.org/10.1016/j.matdes.2024.112681
12. Guo S, Zhao Y, Lin F, et al. (2025) Steady-state rolling resistance prediction model of non-pneumatic tyres considering tread temperature: theory and experiment. *Veh Syst Dyn* 63: 876–896. https://doi.org/10.1080/00423114.2024.2362382
13. Liu S, Liu W, Zhou S, et al. (2023) Steady-state temperature field and rolling resistance characteristics of low-speed and low-load capacity non-pneumatic tires. *Lubricants* 11: 402. https://doi.org/10.3390/lubricants11090402
14. Zhu X, Pang Y, Yang J, et al. (2022) Numerical analysis of hydroplaning behaviour by using a tire–water-film–runway model. *Int J Pavement Eng* 23: 784–800. https://doi.org/10.1080/10298436.2020.1774587
15. Cattani P, Cattani L, Magrini A (2023) Tyre–road heat transfer coefficient equation proposal. *Appl Sci* 13: 11996. https://doi.org/10.3390/app132111996
16. He H, Liu J, Zhang Y, et al. (2022) Heat build-up and rolling resistance analysis of a solid tire: Experimental observation and numerical simulation with thermo-mechanical coupling method. *Polymers* 14: 2210. https://doi.org/10.3390/polym14112210
17. Wyatt O, Chatzistergos P, Chockalingam N, et al. (2024) A flexible-spoke non-pneumatic tyre for manual wheelchairs. *Sci Rep* 14: 29032. https://doi.org/10.1038/s41598-024-79689-1
18. Zheng Z, Dorugade D, Rakheja S, et al. (2024) Multi-axis and cornering stiffness properties of non-pneumatic wheels with symmetric helical honeycomb spokes. *Proc Inst Mech Eng Part D* 238: 3007–3025. https://doi.org/10.1177/09544070231182769
19. Fazelpour M, Summers JD (2014) Evolution of meso-structures for non-pneumatic tire development: A case study. Proceedings of the ASME 2014 International Design Engineering Technical Conferences and Computers and Information in Engineering Conference. Volume 2B: 40th Design Automation Conference, Buffalo, New York, USA, August 17–20. https://doi.org/10.1115/DETC2014-34184

20. Wang J, Zeng H, Gao Q, et al. (2024) Fatigue life prediction and structural optimization design of the bionic petal non-pneumatic tire with spokes. *Proc Inst Mech Eng Part D* 238: 4569–4580. https://doi.org/10.1177/09544070231197585
21. Fu H, Wang Y, Chen K, et al. (2024) A fatigue life prediction model of flexible spoke non-pneumatic tires. *Eng Fract Mech* 295: 109795. https://doi:10.1016/j.engfracmech.2023.109795
22. Jo H, Lee C, Kim K, et al. (2013) Vibration characteristics of non-pneumatic tire with honeycomb spokes. *Trans Korean Soc Automot Eng* 21: 174–180. https://doi.org/10.7467/KSAE.2013.21.4.174
23. Tanveer M, Zu JW (2012) Non-linear vibration of hyperelastic axisymmetric solids by a mixed p-type method. *Int J Non-Linear Mech* 47: 30–41. https://doi.org/10.1016/j.ijnonlinmec.2011.08.003
24. Wu X, Chen Q, Zhao B, et al. (2023) Safety assessment of aircraft panel under the impact load by tire fragment based on thermal–mechanical effect. *J Mater Eng Perform* 32: 1119–1132. https://doi.org/10.1007/s11665-022-07180-x
25. Eck S, Prevedel P, Marsoner S, et al. (2014) Using finite element simulation to optimize the heat treatment of tire protection chains. *J Mater Eng Perform* 23: 1288–1295. https://doi.org/10.1007/s11665-013-0854-y
26. Liu X, Cai J, Zeng J, et al. (2021) Analysis of CFRP laminates properties under different layup structure using finite element analysis. *Mater Res Proc* 18: 249–254. https://doi.org/10.21741/9781644901311-30
27. Mohd Sabee SSN, Yusof N, Rasid ZA, et al. (2021) Progressive failure analysis of laminated composite plates. *IOP Conf Ser Mater Sci Eng* 1051: 012041. https://doi.org/10.1088/1757-899X/1051/1/012041
28. Li F, Hu X, Shahzad Q (2025) Anisotropic behavior in 3D printed concrete: Finite element simulation approach. *J Mater Eng Perform* 34: 8848–8859. https://doi.org/10.1007/s11665-024-10536-0
29. Soliman ESMM (2021) Evaluation of modal parameters and static characteristics for composite mono leaf spring. *Noise Vib Worldwide* 52: 33–47. https://doi.org/10.1177/0957456520964880
30. Wang L, Wang Z (2020) Failure analysis of the longitudinal composite leaf spring. *J Fail Anal Preven* 20: 1437–1444. https://doi.org/10.1007/s11668-020-00961-3
31. Bounjoum Y, Hamlaoui O, Hajji MK, et al. (2024) Exploring damage patterns in CFRP reinforcements: Insights from simulation and experimentation. *Polymers* 16: 2057. https://doi.org/10.3390/polym16142057
32. Singh B, Mohanty A (2022) Influence of nanodiamonds on the mechanical properties of glass fiber-/carbon fiber-reinforced polymer nanocomposites. *J Mater Eng Perform* 31: 3847–3858. https://doi.org/10.1007/s11665-021-06469-7
33. Ascione F, Maselli G, Nesticò A (2024) Sustainable materials selection in industrial construction: A life-cycle based approach to compare the economic and structural performances of glass fibre reinforced polymer (GFRP) and steel. *J Clean Prod* 475: 143641. https://doi.org/10.1016/j.jclepro.2024.143641
34. Veerakumar VGS, Shanmugavel BP, Paskaramoorthy R, et al. (2021) The influence of graphene nanoplatelets on the tensile and impact behavior of glass-fiber-reinforced polymer composites. *J Mater Eng Perform* 30: 596–609. https://doi.org/10.1007/s11665-020-05335-2

35. Jones RM (1999) *Mechanics of Composite Materials*, 2nd Eds., Boca Raton: CRC Press. https://doi.org/10.1201/9781498711067
36. Shokrieh MM, Rezaei D (2003) Analysis and optimization of a composite leaf spring. *Compos Struct* 60: 317–325. https://doi.org/10.1016/S0263-8223(02)00349-5
37. ANSYS Inc (2024) ANSYS composite preppost failure analysis user's guide, release 2024R1. ANSYS Inc. Available from: https://ansyshelp.ansys.com/account/secured?returnurl=/Views/Secured/corp/v241/en/acp_users_guide/acp_users_guide.html.

AIMS Press